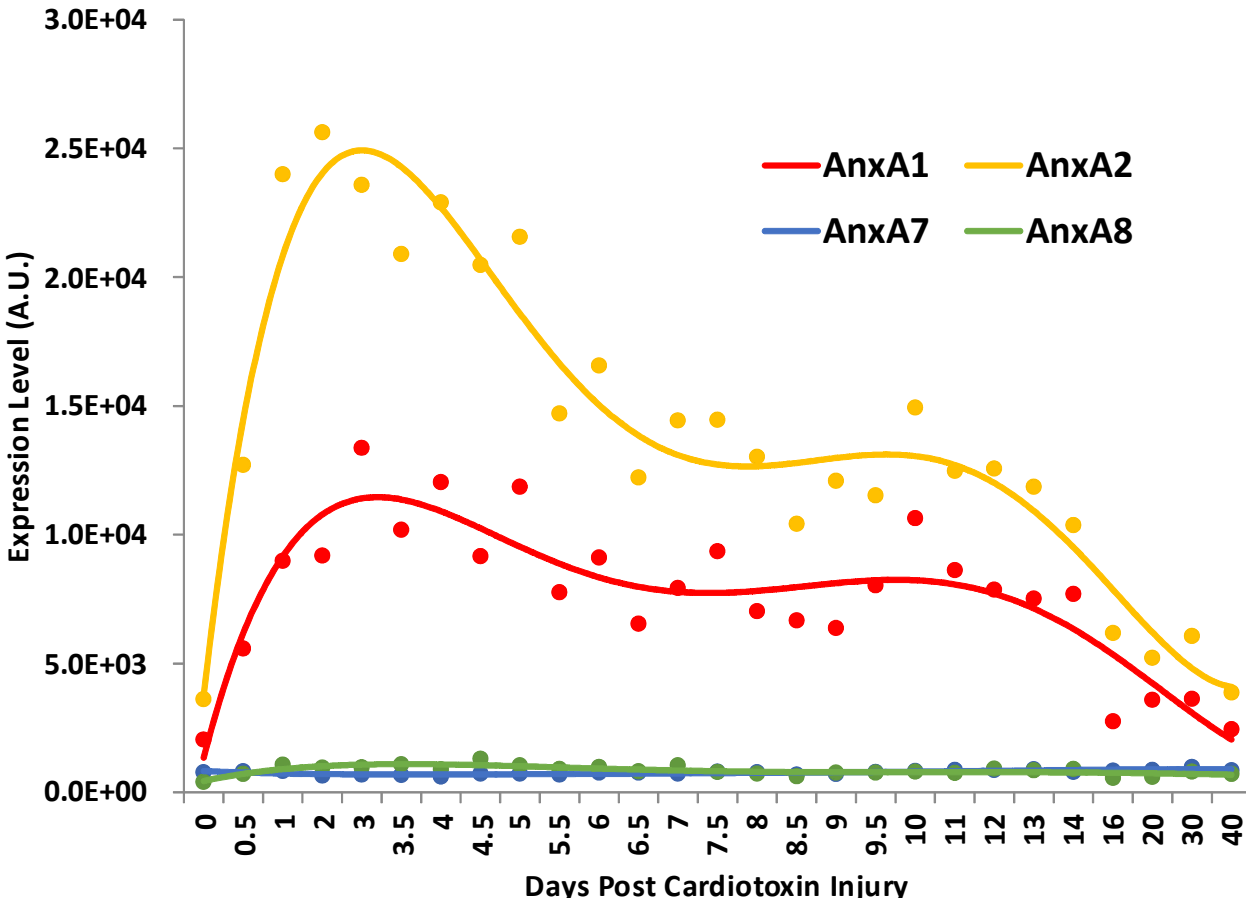

Supplemental Figure 1: Plot showing temporal expression of select Annexin genes during the series of 27 time points following cardiotoxin-injury of *Gastrocnemius* muscle in WT mice that was previously published (14) and publicly available through **Public Expression Profiling Resource at** http://pepr.cnmcresearch.org/.

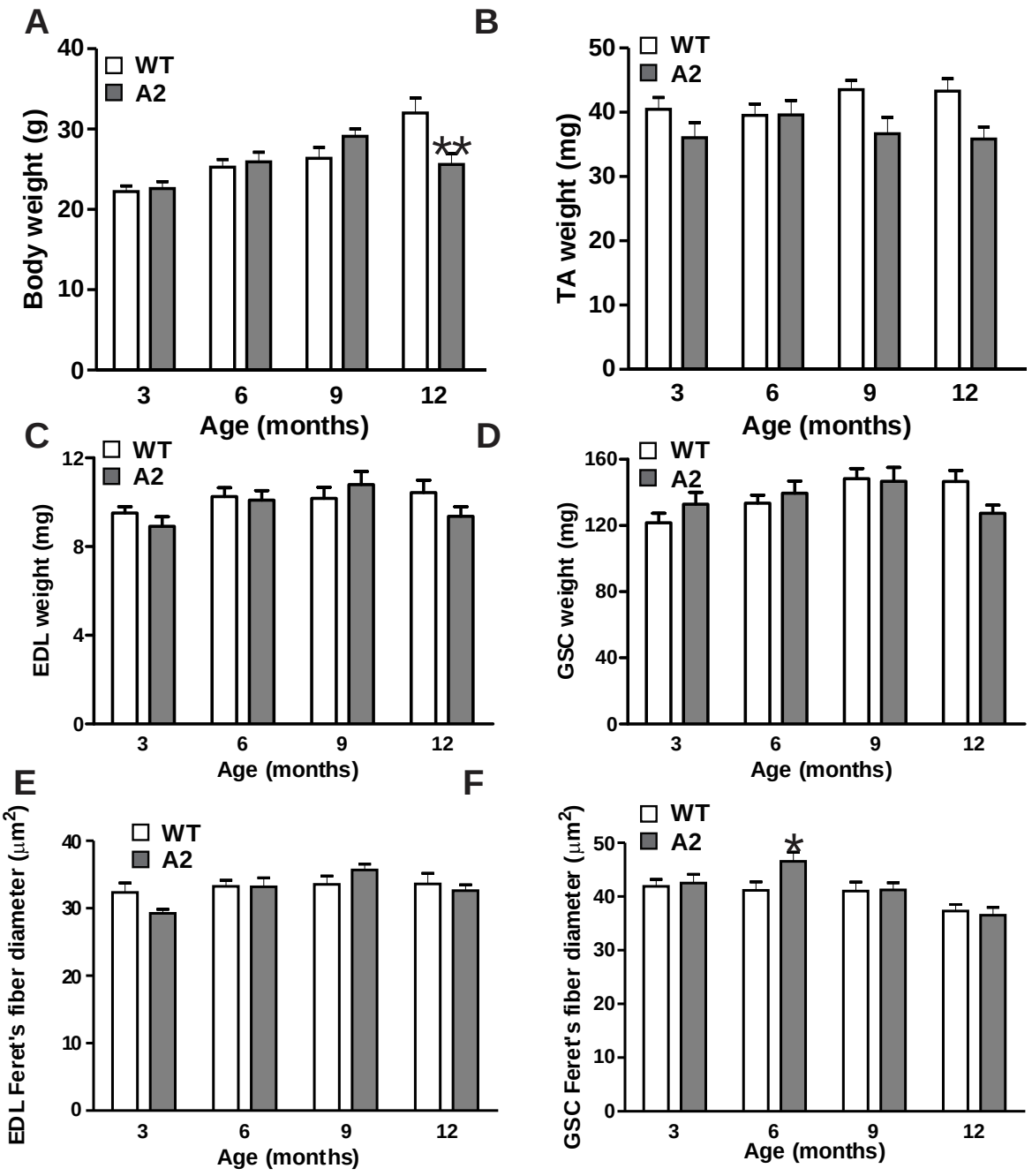

Supplemental Figure 2: WT and A2 mice at 3, 6, 9 and 12 months of age were assessed for **(A)** body mass and **(B-D)** muscle mass (*Tibialis Anterior*, TA, *Extensor Digitorum Longus, EDL and Gastrocnemius*, GSC). Fibers feret's diameter was measured in **(E)** EDL (*Extensor Digitorum Longus*) and **(F)** GSC (*Gastrocnemius*) fibers in WT and A2 animals at 3, 6, 9 and 12 months. All data are expressed as means ± S.E.M. * $p \leq 0.05$ and ** $p \leq 0.01$ compared to WT by ANOVA.

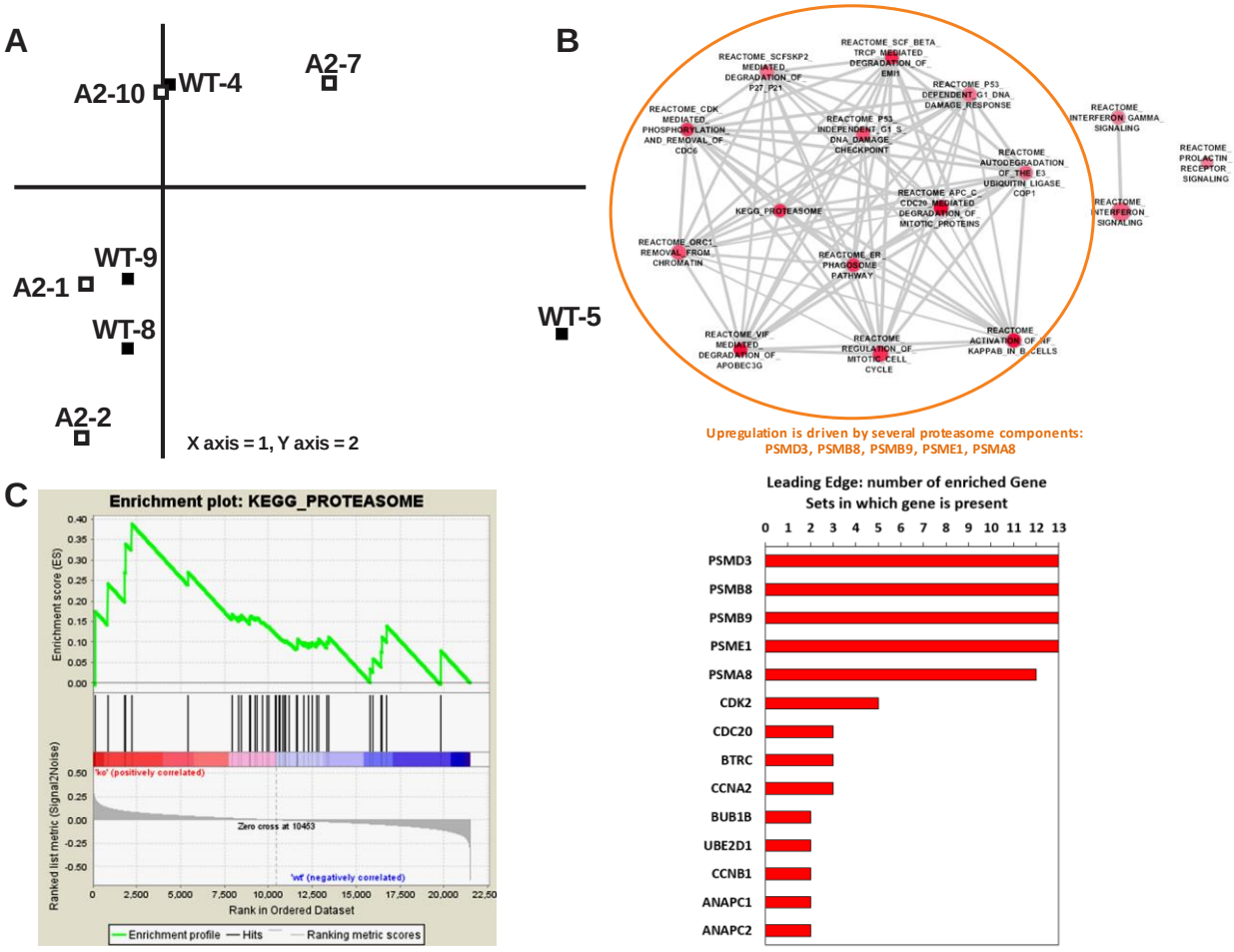

Supplemental Figure 3: (A) Principal component analysis of transcriptome expression matrix of muscle samples from A2 and WT mice. A2 samples do not cluster separately from wild-type, indicating that the global profiles of these mice do not differ. Microarray gene expression data were subjected to quality control and Robust Multi-Array (RMA) normalization. **(B)** Of the 16 gene sets that were up-regulated in the A2, 13 of these showed considerable overlap of genes. These 13 are circled in the enrichment map here (upper panel). 37 genes were shared by these 13 and all encode proteasome components (indicated by first arrow). 5 of these proteasomal genes were present in the leading edges (the leading edge is the part of the gene set distribution that drives its enrichment) of 12 of the 13 gene sets, indicating that just these 5 genes are responsible for the enrichment of all 13 of the proteasome-related gene sets. Other proteasome-related genes are not dysregulated, instead being distributed in the center when the transcriptomic profile is ranked by fold-change. **(C)** Black bars indicate positions of individual proteasome genes within the transcriptome profile; green graph line indicates derivation of enrichment score.

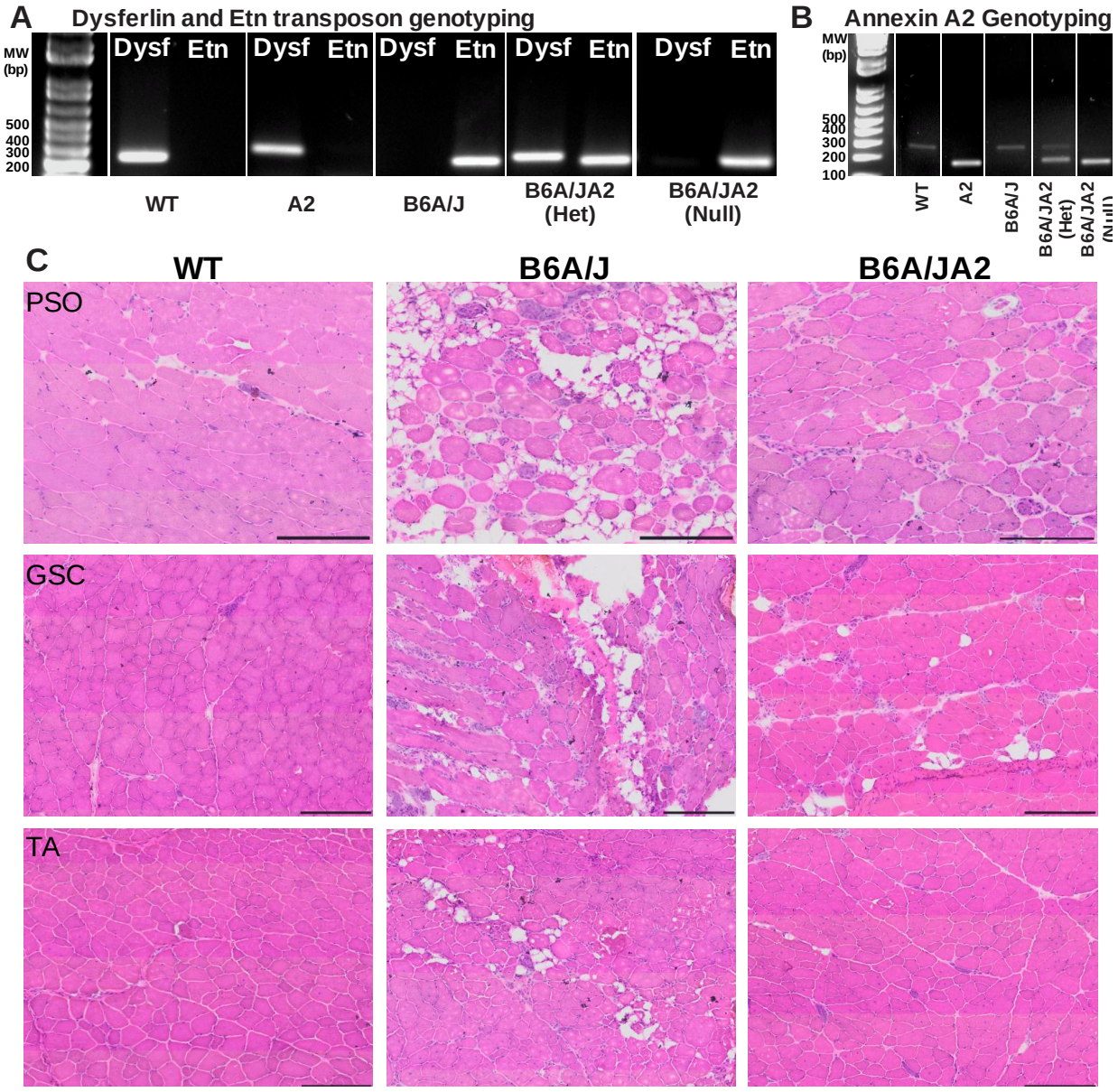

Supplemental Figure 4: (A) PCR analysis of genomic DNA from WT, A2, B6A/J or B6A/JA2 (heterozygote - het; null - B6A/JA2) mice to assess full-length dysferlin allele (Dysf), and insertion of the Etn retrotransposon (Etn) in the dysferlin gene. **(B)** PCR analysis of genomic DNA from WT, A2, B6A/J or B6A/JA2 (heterozygote or null B6A/JA2) mice in order to identify the presence of the AnxA2 gene **(C)** Representative haematoxylin & eosin-stained sections of the *Psoas* (PSO), *Gastrocnemius* (GSC) and *Tibialis Anterior* (TA) from 24 month-old WT, B6A/J and B6A/JA2. Scale = 200µm.

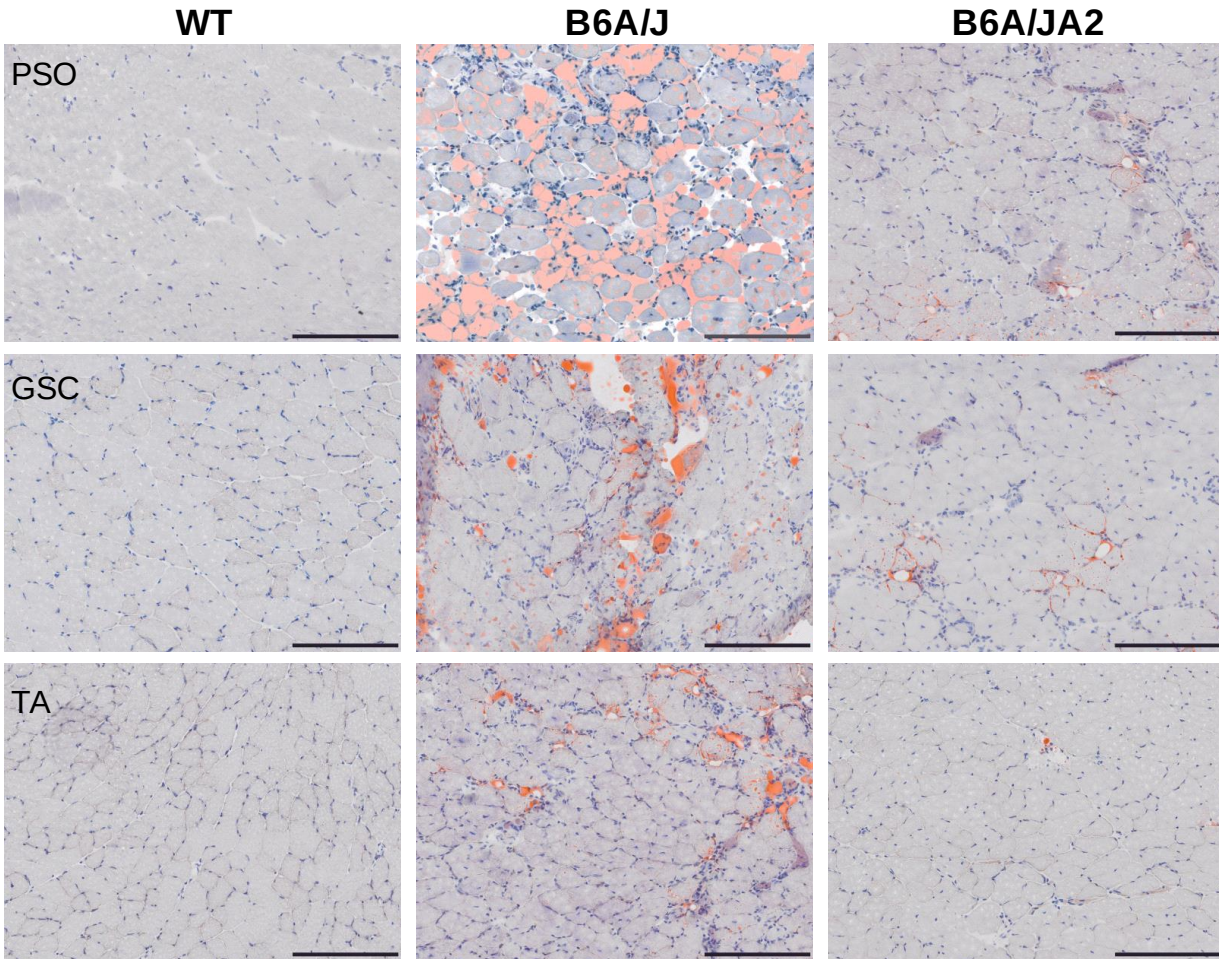

Supplemental Figure 5: Representative Oil Red O-stained sections of the *Psoas* (PSO), *Gastrocnemius* (GSC) and *Tibialis Anterior* (TA) from 24 month-old WT, B6A/J and B6A/JA2. Scale = 200µm.

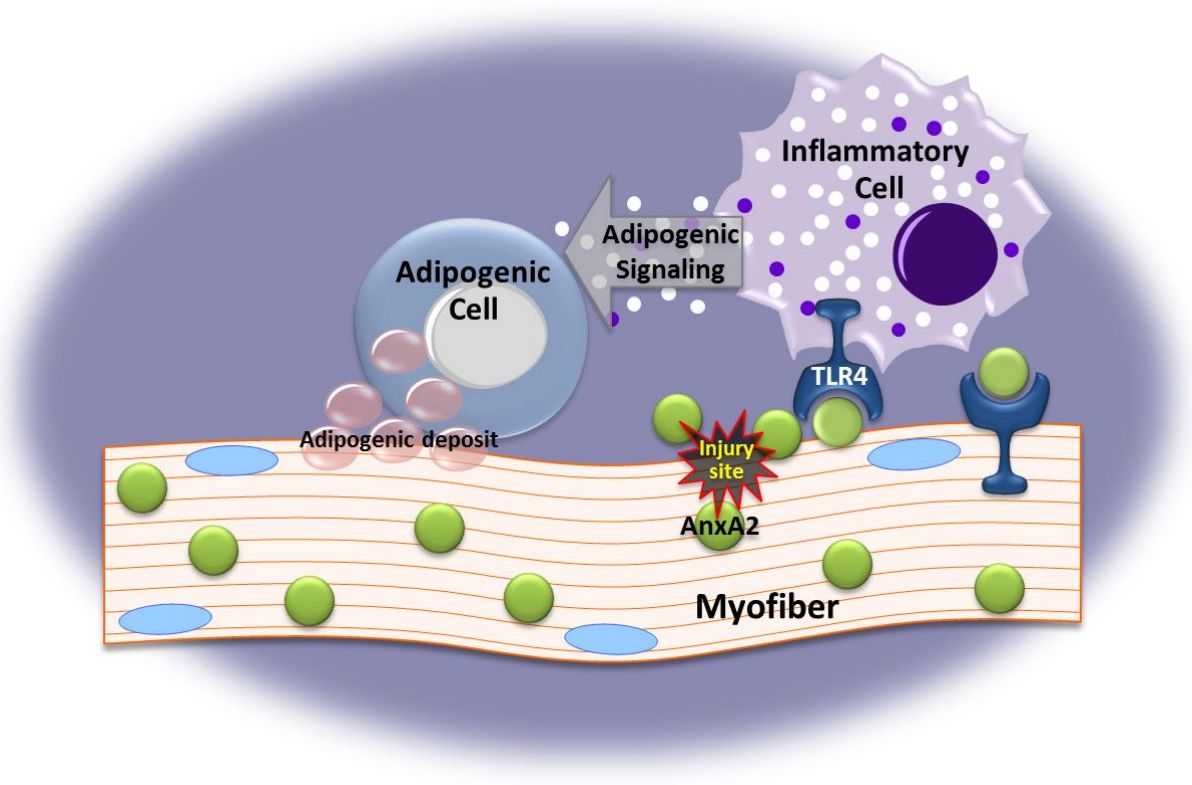

Supplemental Figure 6: Proposed model of Annexin A2-mediated adipogenic replacement of dysferlinopathic myofibers. Intracellular AnxA2 aids in the repair of sarcolemmal injury and is also released during the repair process. Once extracellular, AnxA2 interacts with TLR4 on the muscle and inflammatory cell surface to activate local inflammatory response. While this signaling is normally beneficial, excess production and release of AnxA2 due to poor repair of dysferlin-deficient myofiber or due to myofiber necrosis causes chronic inflammation and downstream signaling that activates adipogenic response that results in adipogenic replacement of myofibers with age and causes increased severity of disease in dysferlinopathic mice and patients.